Journal of Solid State Chemistry **152,** 332–339 (2000)
doi:10.1006/jssc.2000.8652, available online at http://www.idealibrary.com on IDEAL®

Crystal Structure of $Cu_2Gd_{2/3}S_2$: Interlayer Short-Range Order of Gd Vacancies

Mitsuko Onoda,[1] Xue-an Chen,[2] Akira Sato, and Hiroaki Wada

National Institute for Research in Inorganic Materials, Namiki 1-1, Tsukuba, Ibaraki, 305-0044, Japan

Received August 24, 1999; in revised form February 10, 2000; accepted February 18, 2000

The average structure of ternary sulfide $Cu_2Gd_{2/3}S_2$ has been refined using single-crystal X-ray diffraction data: space group $P\bar{3}$, $a = b = 3.899(1)$, $c = 6.421(2)$ Å, $Z = 1$, $R_F = 0.036$, and $wR_F = 0.041$ for 418 reflections and 8 structural parameters. The average structure is based on hexagonal close packing of S with Cu in tetrahedral sites and Gd in octahedral sites, the latter sites being occupied to 2/3. Diffuse streaks observed by electron diffraction, however, indicate a trigonal strict periodicity of $A = 6.753$ Å $= \sqrt{3}a$ within (001) and a vague period of $C = 12.842$ Å $= 2c$, suggesting a layer structure with an intralayer order and interlayer short-range order of Gd vacancies. A model of the real structure has been proposed, and the diffuse scattering has been simulated by the matrix method for one-dimensional disorder. The calculated intensity distribution corresponds to the observed distribution of the diffuse streaks in the electron diffraction pattern and to the intensity distribution measured on an X-ray single-crystal diffractometer; the total X-ray powder diffraction pattern of $Cu_2Gd_{2/3}S_2$ can be reproduced almost completely by calculation.

Key Words: **$Cu_2Gd_{2/3}S_2$; electron diffraction; X-ray diffraction; crystal structure; defects.**

INTRODUCTION

The systems Cu–*R*–S (*R* = the heavy lanthanides) have been studied by Ballestracci *et al.* (1, 2), Julien-Pouzol *et al.* (3–5), Dismukes *et al.* (6), and Aliev *et al.* (7, 8). A trigonal solid solution phase in the range from $CuRS_2$ to $Cu_2R_{2/3}S_2$ has been reported. The structure of $Cu_2Er_{2/3}S_2$ was determined by Ballestracci *et al.* (1, 2) using the X-ray powder diffraction pattern. In the trigonal $P\bar{3}$ cell with $a = 3.9$ and $c = 6.4$ Å, the Cu atoms are in the tetrahedral sites among the hexagonal closest packed S atoms, and the *R* atom with an occupation factor 2/3 has a nearly regular octahedral environment of sulfur atoms. Though confirmation of the presence or absence of superstructure had been left as a problem to be solved for a long time (9), rather recently electron microscopic observation of $Cu_2Er_{2/3}S_2$ has shown long-range order of vacancies in layers and the stacking of these layers more or less random (10).

In the Cu–Gd–S system, single crystals of $Cu_2Gd_{2/3}S_2$ have been prepared in our laboratory. After the measurement of X-ray diffraction from a single crystal using an automatic diffractometer, the diffraction pattern seems to be assigned based on a trigonal unit cell with lattice constants $A = 6.753(1) = \sqrt{3} \times 3.899$ and $C = 12.842(3) = 2 \times 6.421$ Å and it seems to suggest the presence of superstructure due to the ordering of Gd and vacancies. In the X-ray powder diffraction pattern of $Cu_2Gd_{2/3}S_2$, however, no superreflection but a rise in the background level is observed. Furthermore, diffuse streaks on an electron diffraction pattern of $Cu_2Gd_{2/3}S_2$ are observed. All strong reflections can be indexed based on a basic cell with $a = 3.899$, $c = 6.421$ Å, and they suggest that the average structure of $Cu_2Gd_{2/3}S_2$, in which Gd and vacancies are assumed to be distributed randomly in octahedral sites, is isomorphous to that of $Cu_2Er_{2/3}S_2$ (1, 2, 9).

In the present paper, the results of structure refinement of the average structure are described first. Next, an intralayer order and interlayer short-range order model is proposed and examined by application of the matrix method which has been used for one-dimensional disorder (11–15).

EXPERIMENTAL

Single crystals of $Cu_2Gd_{2/3}S_2$ were prepared by chemical transport reaction in an evacuated quartz tube, using a 1000-mg stoichiometric mixture of Cu_2S, Gd, and S, all with nominal purity greater than 99.9%, and 10 mg of iodine as the transport agent. The sample was kept for two weeks under a temperature gradient from 1173 to 1073 K. After quenching in cold water, the gray hexagonal plate-like crystals of metallic luster were obtained in about 60% yield at the cool end of the quartz tube. Direct reaction of pellets of a stoichiometric mixture of elements at 1173 K for two

[1] To whom correspondence should be addressed. E-mail: onodam@nirim.go.jp.

[2] Present address: Department of Chemistry, Rutgers University, Camdem, NJ 08102.

0022-4596/00 $35.00

weeks yielded an almost single-phase sample with few impurities as confirmed by the results of powder X-ray analysis to be described below. The chemical composition of the crystals was determined by means of a JEOL JXA-8600 MX electron microprobe, using $Gd_3Ga_5O_{12}$ and $CuFeS_2$ as standards for Gd, Cu, and S, respectively. An approximate atomic ratio Cu:Gd:S = 3.1:1.0:3.0 was obtained, consistent with that deduced from the structural refinement.

The crystal fragments were obtained by crushing, and electron diffraction patterns were taken using a 100-kV electron microscope (JEOL-1010). The X-ray diffraction data from the powdered specimen were collected with a step-scan procedure, step size 0.02° and sample time 15 s, on a Rigaku-RAD-2B-type diffractometer using Cu$K\alpha$ radiation with a counter-side graphite monochromater. The X-ray diffraction data were collected from a single crystal with an Enraf–Nonius CAD4 automatic diffractometer using graphite monochromatized Mo$K\alpha$ radiation. They were assigned based on a trigonal unit cell with lattice constants $A = 6.753 = \sqrt{3} \times 3.899$ and $C = 2 \times 6.421$ Å. The intensity data were corrected for Lorentz and polarization effects and for absorption by a Gaussian numerical integration using the measured dimensions of the crystal, $0.18 \times 0.14 \times 0.05$ mm. Some measurement conditions are summarized in Table 1.

Measurement of X-ray diffuse scattering has been performed by ω-scan with the Enraf–Nonius CAD4 diffractometer according to information from electron diffraction experiments.

TABLE 1
Conditions of Data Collection and Reduction for $Cu_2Gd_{2/3}S_2$

Chemical formula	$Cu_2Gd_{2/3}S_2$
Formula weight	296.04
Crystal dimension (mm)	$0.18 \times 0.14 \times 0.05$
Unit cell for data collection	
A (Å)	6.753(1)
C (Å)	12.842(3)
Z	6
Calculated density (Mg m^{-3})	5.815
Temperature of data collection (K)	293
Wavelength λ (Mo$K\alpha_1$) (Å)	0.70930
Linear absorption coefficient μ (mm^{-1})	26.37
Transmission factors	0.057–0.277
Scan type	ω–2θ
2θ (max)	80°
Reflections including diffuse streaks	
Range in HKL based on the large cell ($A = 6.753$, $C = 12.842$ Å)	0–10, 0–10, ±23
Total number of reflections measured	2486
Main reflections assigned to the basic cell ($a = 3.899$, $c = 6.421$ Å)	
Total number	418
Number of those with $I > 3\sigma(I)$	418
$R_{int}(F)$	0.020

RESULTS

Structure refinement of the Average Structure

Only reflections with HKL (H–$K = 3n$ and $L = 2n$) have been used to refine the average structure of $Cu_2Gd_{2/3}S_2$, because investigations of diffraction data have revealed that the reflections with HKL (H–$K \neq 3n$ or $L \neq 2n$) are affected by disorder. Using the vector relations $\mathbf{a}_1 = (2\mathbf{A}_1 + \mathbf{A}_2)/3$, $\mathbf{a}_2 = (-\mathbf{A}_1 + \mathbf{A}_2)/3$, and $\mathbf{c} = \mathbf{C}/2$, the average structure is described based on a trigonal unit cell with $a = 3.899$, $c = 6.421$ Å, $Z = 1$. In the present paper, HKL and hkl are used for the indexes, respectively, based on $\mathbf{A}_1$, $\mathbf{A}_2$, and $\mathbf{A}_3$ and based on $\mathbf{a}_1$, $\mathbf{a}_2$, and $\mathbf{a}_3$, and the relations between the indexes are $h = (2H + K)/3$, $k = (-H + K)/3$, and $l = L/2$. Refinement was performed on the basis of $|F|$ through the computer program FMLSM (16–18) with unit weight for all reflections, assuming space group $P\bar{3}$ and twinning about [001] with twin operation $-x, -y, z$. All of the 418 main reflections assigned based on the basic cell ($a = 3.899$, $c = 6.421$ Å) were used, because each of them has $\sigma(I)$ smaller than one third of measured intensity I. In the early stages, the occupation factor of Gd was allowed to vary. As the resulting occupancy of Gd was 0.665(5) and was within one standard deviation of the ideal occupancy 2/3, the ideal occupancy of Gd was assumed in the final stage. The agreement was satisfactory with 8 structural parameters (2 positional parameters and 6 anisotropic thermal parameters) and 2 scale factors and 1 extinction correction parameter incorporated in FMLSM; $R_F = 0.036$ and $wR_F = 0.041$. The final structural parameters are listed in Table 2. The final F-based scale factors are 37.4(3) and 28.1(2), and they correspond to the volume ratio 1.77(5):1 of twin domains, and the parameter for extinction correction is $4.1(4) \times 10^{-6}$. Listings of the structure factors are available from the authors.

X-Ray Powder Diffraction Pattern and Rietveld Analysis

The X-ray powder diffraction pattern of $Cu_2Gd_{2/3}S_2$ is shown in Fig. 1 with indices HKL based on the basic cell ($a = 3.899$, $c = 6.421$ Å). Except for several peaks due to impurity, which is inferred to be Gd_2O_2S (19) from careful assignment of the powder pattern, all sharp reflections can be indexed on the basic cell. Diffuse scattering is observed as a rise of background level around the positions of $d = 5.32$, 2.85, and 2.18 Å, close to the superreflection positions based on a cell with $A = 6.753 = \sqrt{3} \times 3.899$ and $C = 2 \times 6.421$ Å. Rietveld analysis of the average structure was performed as shown in Fig. 2 using the computer program RIETAN (20, 21) in which peak shapes are expressed by the pseudo-Voigt function (22) with asymmetry correction (23). A two-phase refinement was performed in order to account for the presence of 4.8(4)%(w/w) Gd_2O_2S on the assumption that Gd_2O_2S is isomorphous to La_2O_2S (24)

TABLE 2
Atomic Parameters of the Average Structure Based on the Trigonal Cell with $a = 3.899$ and $c = 6.421$ Å with Estimated Standard Deviations in Parentheses

Atom	x	y	z	U_{11}	U_{12}	U_{13}	U_{22}	U_{23}	U_{33}	U_{eq}
Gd*	0	0	0	0.0191(6)	0.0096	0.0	0.0191	0.0	0.035(1)	0.0244(4)
Cu	1/3	2/3	0.3698(2)	0.048(1)	0.024	0.0	0.048	0.0	0.081(2)	0.059(1)
S	2/3	1/3	0.2523(3)	0.022(1)	0.011	0.0	0.022	0.0	0.038(3)	0.027(1)

Note. The anisotropic displacement factor exponent takes the form $-2\pi^2(h^2a^{*2}U_{11} + 2hka^*b^*U_{12} + 2hla^*c^*U_{13} + k^2b^{*2}U_{22} + 2klb^*c^*U_{23} + l^2c^{*2}U_{33})$. $U_{eq} = B_{eq}/(8\pi^2) = (1/3)[(\mathbf{a}, \mathbf{a})a^{*2}U_{11} + (\mathbf{b}, \mathbf{b})b^{*2}U_{22} + (\mathbf{c}, \mathbf{c})c^{*2}U_{33} + 2(\mathbf{b}, \mathbf{c})b^*c^*U_{23}]$.
* Occupation number of Gd is 2/3 (see text).

with space group $P\bar{3}m1$. The agreement, $R_{WP} = 0.061$, $R_P = 0.044$, $R_B(Cu_2Gd_{2/3}S_2) = 0.045$, $R_F(Cu_2Gd_{2/3}S_2) = 0.027$, $R_B(Gd_2O_2S) = 0.036$, $R_F(Gd_2O_2S) = 0.019$, and $R_E = 0.020$ with 123 reflections and 35 parameters including 6 parameters for the background approximated by a sum of Legendre polynomials, was acceptable, because background was considered to be affected by diffuse scattering. The cell dimensions and the atomic parameters of $Cu_2Gd_{2/3}S_2$ obtained were $a = 3.8986(7)$, $c = 6.430(1)$ Å, Gd in (0, 0, 0) with occupation number 2/3, Cu in $\pm(1/3, 2/3, z)$ with $z = 0.369(2)$ and S in $\pm(2/3, 1/3, z)$ with $z = 0.248(4)$ and overall isotropic thermal parameter $B = 0.0(3)$ Å^2, while those of Gd_2O_2S are $a = 3.851(1)$, $c = 6.664(2)$ Å, Gd in $\pm(2/3, 1/3, z)$ with $z = 0.268(1)$, O in $\pm(1/3, 2/3, z)$ with $z = 0.327(4)$, S in (0,0,0), and $B = 0(2)$. In this way, the sharp reflections with indexes in Fig. 1 have been confirmed to come from the average structure shown in Table 2.

The average structure model of $Cu_2Gd_{2/3}S_2$ is illustrated in Fig. 3a using the atomic positions listed in Table 2.

Electron Diffraction Pattern and Measurement of X-Ray Diffuse Scattering

In the electron diffraction pattern with the incident beam perpendicular to the c axis, diffuse streaks appear as shown in Fig. 4. A section of the diffuse streaks indicates the

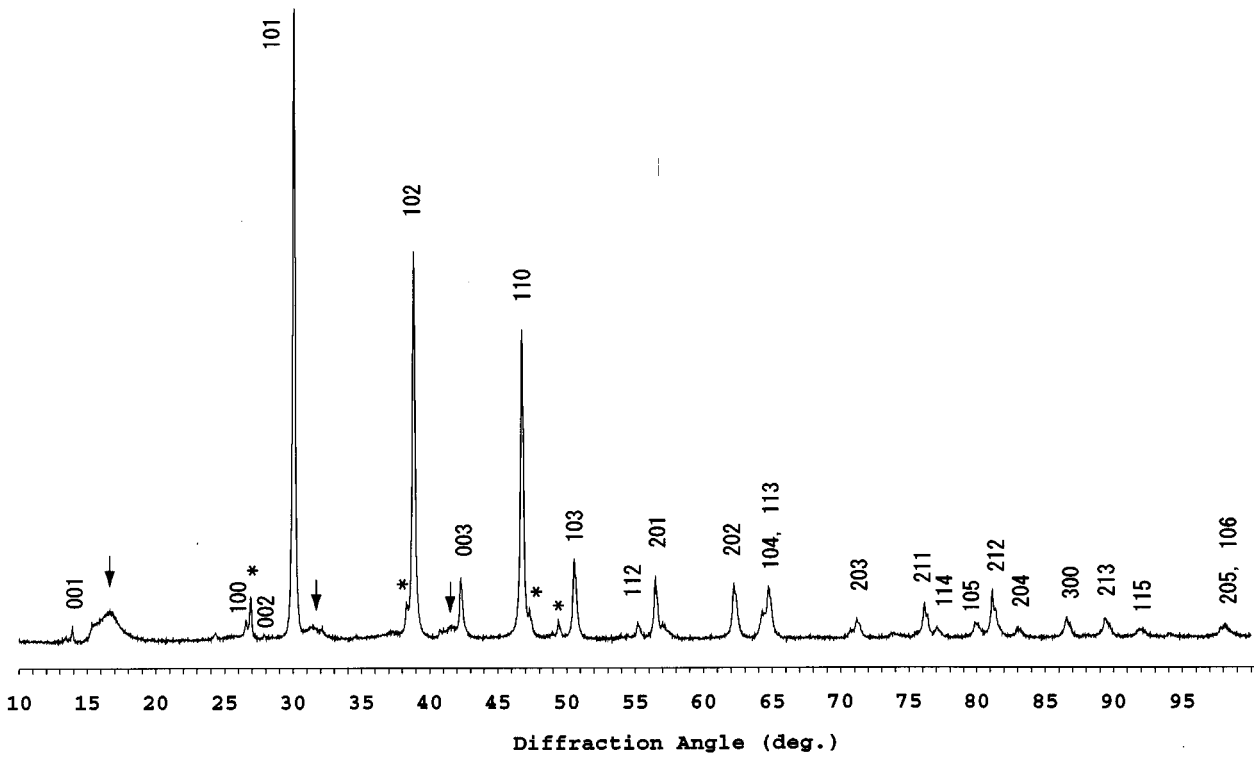

FIG. 1. X-ray powder diffraction pattern of $Cu_2Gd_{2/3}S_2$ for Cu$K\alpha$ radiation. Reflection are assigned based on a trigonal unit cell with $a = 3.899$ and $c = 6.421$ Å. The peaks with asterisks are due to impurity. Rises of background indicated by small arrows (↓) are observed around the superreflection positions based on a trigonal cell with $A = 6.753 = \sqrt{3} \times 3.899$ and $C = 2 \times 6.421$ Å.

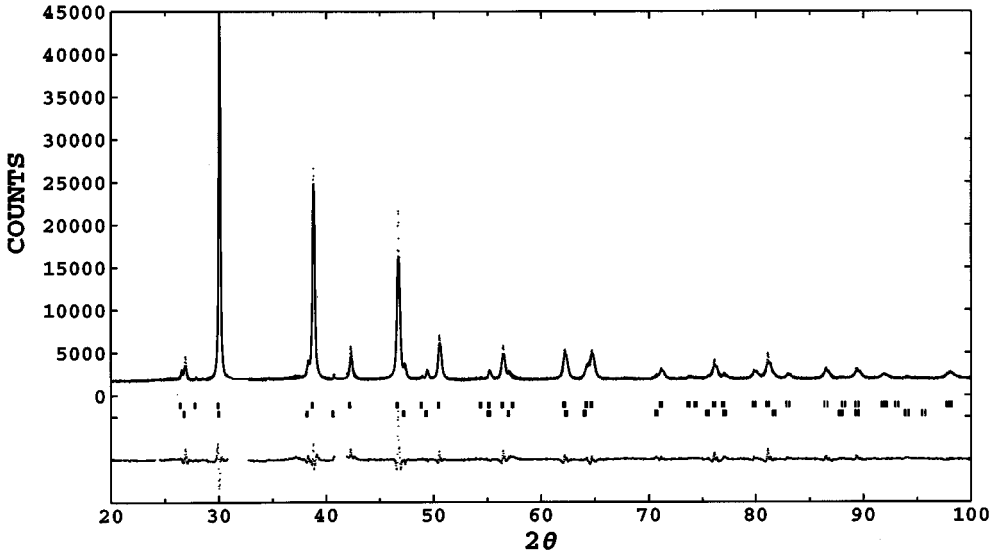

FIG. 2. Rietveld analysis pattern (Cu$K\alpha$) of the average structure of $Cu_2Gd_{2/3}S_2$. Vertical lines, upper and lower, show, respectively, the reflection positions of $Cu_2Gd_{2/3}S_2$ and impurity Gd_2O_2S, and the solid line at the bottom of the figure indicates the difference between the observed and calculated intensities.

trigonal cell with $A = \sqrt{3}a$, and this trigonal cell arises from an intralayer order of Gd vacancies. When the trigonal supercell of $\sqrt{3}a$ is regarded as a unit cell, reciprocal coordinates of the diffuse streaks are expressed by $HK\zeta$ ($H-K \neq 3n$), e.g. $H = 1$ and $K = 0$.

Measurement of X-ray diffuse scattering has been performed along 10ζ and 20ζ by ω-scan based on a trigonal cell with lattice constants $A = 6.753 = \sqrt{3} \times 3.899$ and $c = 6.421$ Å. Measured intensities are plotted vs ζ using open circles in Fig. 5a.

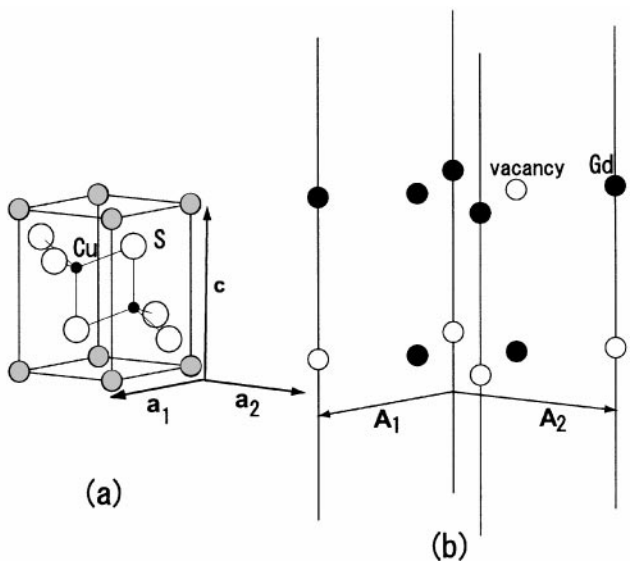

FIG. 3. (a) Average structure model (trigonal: $a = 3.899$, $c = 6.421$ Å) and (b) stacking model of ordered layers of Gd and vacancy (trigonal: $A = \sqrt{3}a$). Relations between the vectors shown above are expressed as $\mathbf{A}_1 = \mathbf{a}_1 - \mathbf{a}_2$, $\mathbf{A}_2 = \mathbf{a}_1 + 2\mathbf{a}_2$. Small solid and large open circles represent Cu and S. Medium solid, shadowed, and open circles represent Gd, partially occupied Gd, and vacancy, respectively. Cu and S are eliminated in (b).

Simulation of Diffuse Scattering Intensities

The diffuse intensity distributions may be examined on the basis of the stacking disorder model. Based on the trigonal cell with $A = \sqrt{3}a$, the structure with an intralayer order of Gd vacancies can be described in terms of the stacking sequence of the layer units whose sizes are expressed by using the vector relations $\mathbf{A}_1 = \mathbf{a}_1 - \mathbf{a}_2$ and $\mathbf{A}_2 = \mathbf{a}_1 + 2\mathbf{a}_2$. All three possible configurations of the layer units, $P1$, $P2$, and $P3$, are shown in Fig. 6, where $P2$ and $P3$ are obtained from $P1$ by shifts of 1/3 and 2/3 in the $[-1\,1\,0]$ direction of the cell with $\mathbf{A}_1$ and $\mathbf{A}_2$. In order to maintain the average structure shown in Fig. 3a, each layer unit ($P1$, $P2$, or $P3$) can be followed by one of $P1$, $P2$, and $P3$. Considering the Coulomb interaction between Gd atoms and vacancies, the sequences such as $P1$–$P1$, in which the neighbor layer units are the same, may be less advantageous than those such as $P1$–$P2$ and $P1$–$P3$ (Fig. 3b). Therefore we have adopted a model of Table 3 with $s = 1$, where s is the number of layer units necessary to distinguish the stacking disorder. In the model, $P1$ is followed by $P2$ and $P3$ with the same probability and so on.

Layer form factors of $P1$ is expressed as

$$V_{P1} = L^{1/2}(\xi, \eta) \left\{ \sum_{i=1}^{2} f_{\mathrm{Gd}} \exp\left[i2\pi(Hx_{\mathrm{Gd}}(i) + Ky_{\mathrm{Gd}}(i) + \zeta z_{\mathrm{Gd}}(\mathrm{i})\right)\right] + \sum_{i=1}^{6} \left[f_{\mathrm{S}} \exp\left[i2\pi(Hx_{\mathrm{S}}(i) + Ky_{\mathrm{S}}(i)\right.\right.$$

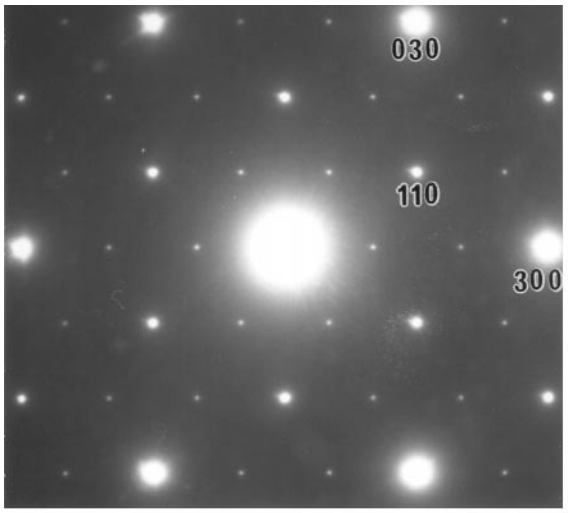

(a)

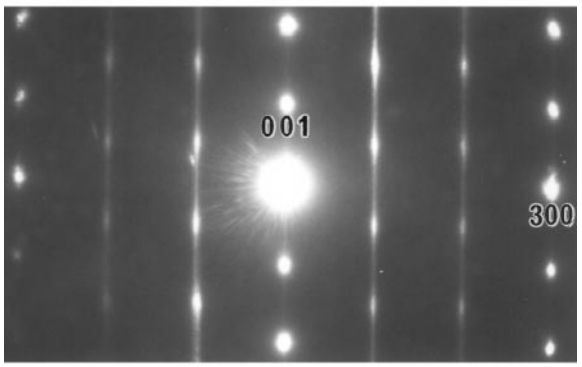

(b)

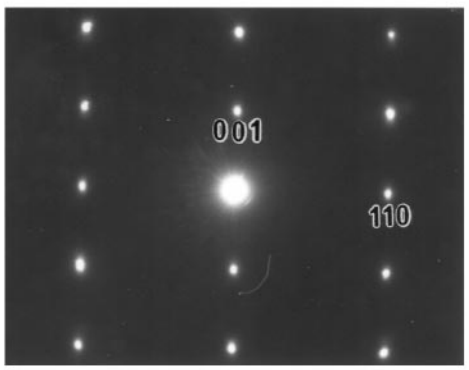

(c)

FIG. 4. Electron diffraction patterns from $Cu_2Gd_{2/3}S_2$. The incident beam is parallel to the (a) [0 0 1], (b) [− 1 1 0], or (c) [0 1 0] of the basic cell (trigonal: $a = 3.899$, $c = 6.421$ Å). Indices (H, K and l) are based on the trigonal cell with $A = 6.753 = \sqrt{3}a$ and $c = 6.421$ Å.

$$+ \zeta z_S(i))] + f_{Cu} \exp[i2\pi(Hx_{Cu}(i) + Ky_{Cu}(i) + \zeta z_{Cu}(i))]\Big\},$$

where $L(\xi, \eta)$ is the Laue function involving $\mathbf{A}_1^*$ and $\mathbf{A}_2^*$; f_{Gd}, f_S, and f_{Cu} are the atomic scattering factors of Gd, S, and Cu atoms; $x(i)$, $y(i)$, and $z(i)$ are the ith coordinates along $\mathbf{A}_1$, $\mathbf{A}_2$ and $\mathbf{c}$; ξ, η, and ζ are the coordinates along $\mathbf{A}_1^*$, $\mathbf{A}_2^*$, and $\mathbf{c}^*$. Layer form factors of $P2$ and $P3$ are given by $V_{P2} = V_{P1}\varepsilon^*$, $V_{P3} = V_{P1}\varepsilon$, where $\varepsilon = \exp[i2\pi(H + K)/3]$ and $\varepsilon^* = \varepsilon^2$.

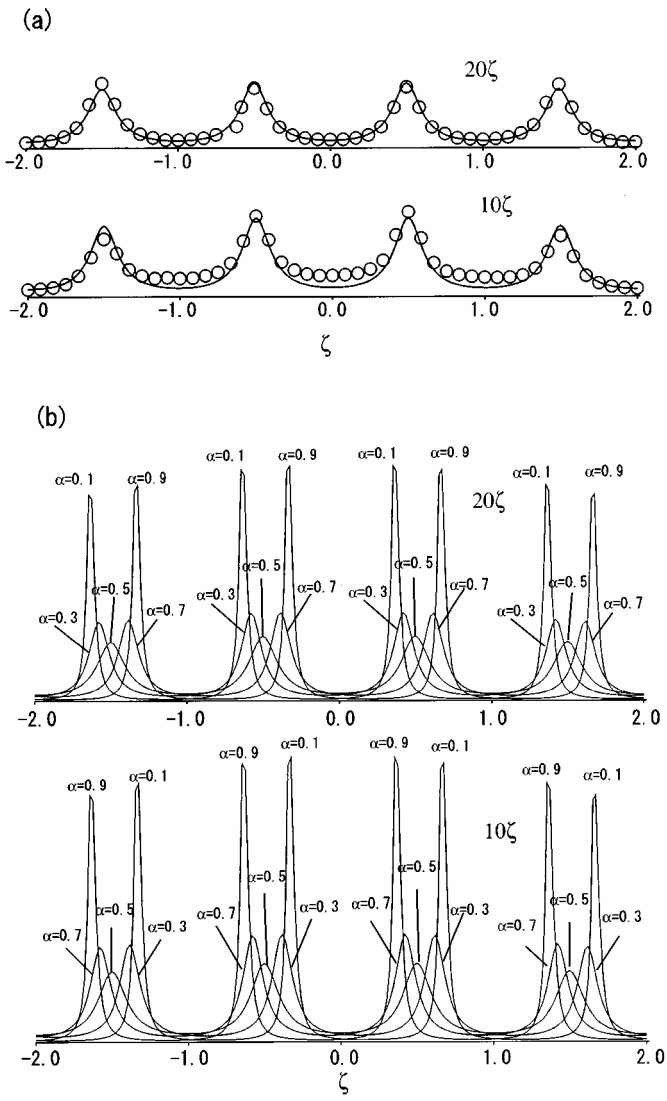

FIG. 5. (a) Intensity distributions of X-ray diffuse scattering corresponding streaks 10ζ (lower) and 20ζ (upper). Open circles represent measured intensities. Calculated intensities for the model of Table 3a are represented by curves. (b) Intensity curves along 10ζ (lower) and 20ζ (upper) lines with various probability values α calculated for the model of Table 3b.

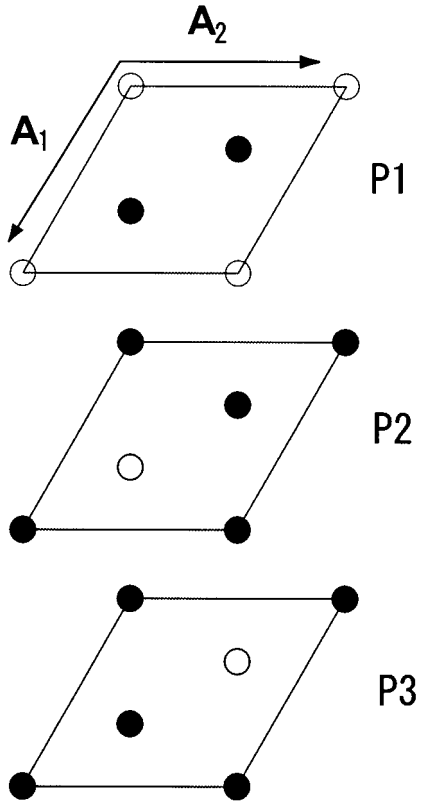

FIG. 6. Possible configurations of Gd and vacancy layer. Solid and open circles represent, respectively, Gd and vacancy.

The scattering intensity from the specimen with stacking disorder is generally given in a matrix form (10, 11) by

$$I(\zeta) = \sum_{m=-(N-1)}^{N} (N - |m|) J_m \exp(-i2\pi m\zeta), \quad J_m = \text{tr } \mathbf{VFP}^m,$$

where N is the total number of layer units, $\mathbf{V}$, $\mathbf{F}$, and $\mathbf{P}$ are matrices and their elements are given by $(\mathbf{V})_{st} = \mathbf{V}_s^* V_t$, $(\mathbf{F})_{ss} = w_s$, $(\mathbf{F})_{st} = 0$ (for $s \neq t$), $(\mathbf{P})_{st} = P_{st}$; w_s is the probability of finding the sth layer unit; P_{st} is the continuing probability of the tth layer unit after the sth layer unit. As the order of matrix becomes 3 in the present model as shown in Table 3, the expression of $I(\zeta)$ deduces to (11–13)

$$I(\zeta)/N = \sum_{v=1}^{3} C_v/[1 - X_v \exp(-i2\pi\zeta)] + \text{conj.} - \sum_{v=1}^{3} C_v,$$

where X_v is the vth eigenvalue of $\mathbf{P}$, C_v is the vth diagonal element of the matrix $\mathbf{Z}^{-1}\mathbf{VFZ}$, when the diagonal form of $\mathbf{P}$ is given by the operation $\mathbf{Z}^{-1}\mathbf{PZ}$.

Using the computer program FV1 (25, 26) based on the above equation, the intensity distribution $I/NL(\xi, \eta)$ was calculated as a function of H, K, and ζ. The results for the model of Table 3a are illustrated as curves in Fig. 5a, and they are in agreement with the measured diffuse scattering intensities represented by open circles.

Simulation of Total X-Ray Powder Diffraction Pattern

The calculation method for intensity distribution in X-ray powder diffraction from a sample with stacking faults was derived (27). The simulation of total X-ray powder diffraction pattern has been attempted on the basis of the stacking model of Table 3. The programs used are FV1 and PPROFL (25, 28). The simulated X-ray powder diffraction pattern is shown in Fig. 7 and it is in good agreement with the experimental pattern shown in Fig. 1 except for impurity peaks.

DISCUSSION

The results of Table 2 and Fig. 3a showed that the average structure is based on hexagonal close packing of S with Cu in tetrahedral sites and Gd in octahedral sites in alternating gaps between S packing layers. The average occupancy of Gd is 2/3. Selected interatomic distances and angles based on the average structure are shown in Table 4, and the values are comparable to those reported in the literature. For example, Cu–S distances of 2.347(2)–2.370(2) Å, and Gd–S distances of 2.731(2)–2.834(1) Å were observed for the four-coordinated Cu and six-coordinated Gd atoms in the $KCuGd_2S_4$ structure (29). The relatively short Cu–Cu distance in Table 4 is considered to be a consequence of edge-sharing of the CuS_4 tetrahedra.

In the model of Table 3a, the sequences such as $P1$–$P1$, in which neighboring order layers are the same, do not occur, and $P1$–$P2$ and $P1$–$P3$ occur with the same probability and

TABLE 3
Probability Table (P Table) Based on the Layer Units Shown in Fig. 6

(a) $P1$–$P1$ is forbidden and $P1$ is followed by $P2$ and $P3$ with the same probability and so on.

	$P1$	$P2$	$P3$
$P1$	0.0	0.5	0.5
$P2$	0.5	0.0	0.5
$P3$	0.5	0.5	0.0

(b) $P1$–$P1$ is forbidden and $P1$ can be followed by $P2$ and $P3$ with different probabilities and so on.

	$P1$	$P2$	$P3$
$P1$	0.0	α	$1-\alpha$
$P2$	$1-\alpha$	0.0	α
$P3$	α	$1-\alpha$	0.0

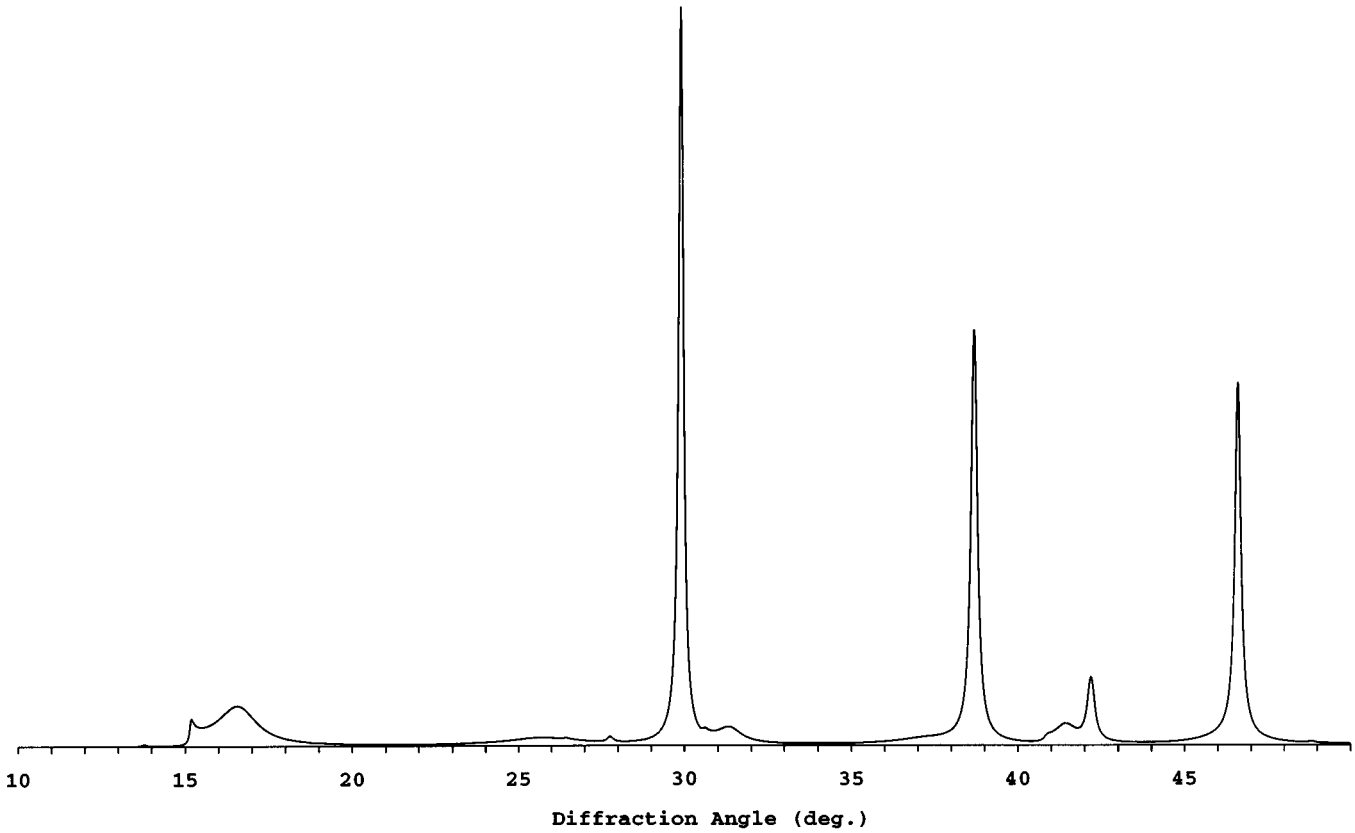

FIG. 7. Calculated X-ray powder diffraction pattern (Cu$K\alpha$).

so on. The distance between the Gd vacancies, that is to say the average distance between ordered Gd sites, belonging to neighboring order layers are longer for $P1$–$P2$ or $P1$–$P3$ than for $P1$–$P1$ and so on. The model is reasonable with respect to the Coulomb interaction between Gd ions and vacancies. The effects of the probability change on the intensity distributions have been examined using the model of Table 3b in which the sequences such as $P1$–$P1$ are forbidden but $P1$ can be followed by different probabilities by $P2$ and $P3$ and so on. The intensity curves along the 10ζ and 20ζ reciprocal-lattice lines calculated for a continuing probability α varying from 0.1 to 0.9 stepwise are illustrated in Fig. 5b. In the case of $\alpha = 0.5$, which expresses the quite same model as Table 3a, the positions of diffuse maxima, $\zeta = n + 1/2$, and the broadness of diffuse streaks agree with those measured as shown in Fig. 5a. As the value of α is away from 0.5, the shape of the diffuse peaks become sharper and the values of ζ of diffuse maxima shift from $n + 1/2$ toward $n + 1/3$ or $n + 2/3$ as shown in Fig. 5b. The simulation results demonstrate that a sequence $P1$–$P1$ is not favorable and $P1$ is followed by $P2$ and $P3$ with the same probability and so on.

TABLE 4
Selected Interatomic Distances (Å) and Angles (°) in the Average Structure of $Cu_2Gd_{2/3}S_2$

Cu–S	2.374(1) × 3	2.426(2) × 1
Cu–Cu	2.804(1) × 3	
S–Cu–S	108.53(3) × 3	110.40(5) × 3
Gd*–S	2.774(1) × 6	
Gd*–Gd*	3.899(1) × 6	
S–Gd*–S	180.00 × 3	90.68(4) × 6

* Occupation number of Gd is 2/3.

The diffuse streaks have been detected in powder X-ray diffraction pattern, Fig. 1 and Fig. 7, and in single-crystal X-ray data as reflections with HKL ($H-K \neq 3n$ or $L \neq 2n$). Index HKL ($H-K \neq 3n$ or $L \neq 2n$) should be replaced by $HK\zeta$ ($H-K \neq 3n$), because the reflections are diffuse due to interlayer short-range order of Gd vacancies. The diffuse maxima in the reciprocal space are observed at the positions $H-K \neq 3n$ or $L \neq 2n$ as shown in Figs. 4 and 5(a), and they are explained by the model of Table 3.

SUMMARY

Single crystals of $Cu_2Gd_{2/3}S_2$ have been prepared. The average structure based on hexagonal close packing of

S with Cu in tetrahedral sites and Gd with average occupancy 2/3 in octahedral sites has been refined using single-crystal X-ray diffraction data: space group $P\bar{3}$, $a = 3.899$, $c = 6.421$ Å, $Z = 1$. Diffuse streaks were observed on an electron diffraction pattern of $Cu_2Gd_{2/3}S_2$ and they show intralayer ordering of Gd and vacancies. An interlayer short-range order model of Gd vacancies was proposed and examined by application of the matrix method for the one-dimensional disorder. The calculated diffuse intensity distribution explains the electron diffraction patterns, measured X-ray diffuse scattering intensities from a single crystal, and the total X-ray powder diffraction pattern of $Cu_2Gd_{2/3}S_2$.

ACKNOWLEDGMENTS

The authors acknowledge K. Kato and F. Izumi for their computer programs and K. Kosuda for carrying out the EPMA analyses. The authors acknowledge K. Kato for valuable advice. One of the authors (X.-A. Chen) acknowledges Japan Science and Technology Corporation for a STA fellowship.

REFERENCES

1. R. Ballestracci and E. F. Bertaut, *C. R. Acad. Sci. Paris* **261,** 5064 (1965).
2. R. Ballestracci and E. F. Bertaut, *Bull. Soc. Miner. Crystallogr.* **88,** 575 (1965).
3. M. Julien-Pouzol, M. Guittard, and C. Adolphe, *C. R. Acad. Sci. Paris, Ser. C* **267,** 823 (1968).
4. M. Julien-Pouzol, M. Guittard, and A. Mazurier, *C. R. Acad. Sci. Paris, Ser. C* **271,** 1317 (1970).
5. M. Julien-Pouzol and M. Guittard, *Ann Chim.* **7,** 253 (1972).
6. J. P. Dismukes, R. T. Smith, and J. G. White, *J. Phys. Chem. Solids* **32,** 913 (1971).
7. U. M. Aliev, R. S. Gamidov, and G. G. Gusejnov, *Izvest. Akad. Nauk, SSSR, Neorg. Mater.* **8,** 1855 (1972).
8. U. M. Aliev, R. S. Gamidov, G. G. Gusejnov, and M. A. Alidzhanov, *Izvest. Akad. Nauk, SSSR, Neorg. Mater.* **9,** 843 (1973).
9. J. Flahaut, *in* "Handbook on the Physics and Chemistry of Rare Earths" (K. A. Gschneidner, Jr., and L. Eyring, Eds.), Vol. 4, Chap. 13, pp. 1–88. North-Holland, Amsterdam, 1979.
10. M. Guymont, A. Thomas, M. Julien-Pouzol, S. Jaulmes, and M. Guittard, *Phys. Status Solidi A* **121,** 21 (1990).
11. S. Hendrics and E. Teller, *J. Chem. Phys.* **10,** 147 (1942).
12. J. Kakinoki and Y. Komura, *Acta Crystallogr.* **19,** 137 (1965).
13. J. Kakinoki, *Acta Crystallogr.* **23,** 875 (1967).
14. M. Onoda and I. Kawada, *Acta Crystallogr. Sect. A* **36,** 134 (1980).
15. M. Onoda, M. Saeki, and I. Kawada, *Acta Crystallogr. Sect. B* **42,** 1 (1986).
16. K. Kato, *Acta Crystallogr. Sect. B* **46,** 39 (1990).
17. K. Kato, *Acta Crystallogr. Sect. A* **50,** 351 (1994)
18. K. Kato, *Z. Kristallogr.* **212,** 423 (1997).
19. Sipe, McCarthy, Penn. State University, JCPDS Grant-in-Aid Report (1974); JCPDS 26–1422.
20. F. Izumi, *in* "The Rietveld Method" (R. A. Young, Ed.), Chap. 13. Oxford University Press, Oxford, 1993.
21. Y.-I. Kim and F. Izumi, *J. Ceram. Soc. Jpn.* **102,** 401 (1994).
22. P. Thompson, D. E. Cox, and J. B. Hastings, *J. Appl. Crystallogr.* **20,** 79 (1987).
23. C. J. Howard, *J. Appl. Crystallogr.* **15,** 615 (1982).
24. B. Morosin and D. J. Newman, *Acta Crystallogr. Sect. B* **29,** 2647 (1973).
25. K. Kato, FV1, personal communication, 1991.
26. K. Kato, K. Kosuda, T. Koga, and H. Nagasawa, *Acta Crystallogr. Sect. C* **46,** 1587 (1990).
27. M. Onoda, M. Saeki, and I. Kawada, *Acta Crystallogr. Sect. A* **36,** 952 (1980).
28. K. Kato, PPROFL, personal communication, 1998.
29. P. Stoll, P. Dürichen, C. Näther, and W. Bensch, *Z. Anorg. Allg. Chem.* **624,** 1807 (1998).